INTERNSHIP FEBRUARY-JUNE 2023

CRYSTALLIZATION OF BIODEGRADABLE THERMOPLASTIC POLYMER (PBS): APPLICATION FOR FUSED FILAMENT FABRICATION

MATERIALS & ENGINEERING SCIENCES IN PARIS - MAGIS
2022-2023

MIRÓ PINA Laura
laura.miro_pina@ensam.eu

TUTOR: Jorge PEIXINHO & Xavier COLIN

REVIEWER: Sébastien ROLAND

PIMM|PROCEDES ET INGENIERIE EN MECANIQUE ET MATERIAUX
151 Bd de l'Hôpital, 75013 Paris

Table of contents

Table of figures

1. Introduction

In recent years, the increasing environmental impact of conventional plastics has generated a growing awareness of the need to find more sustainable alternatives. In this context, biodegradable thermoplastic polymers have emerged as a promising solution to address this challenge (Kunioka, Ninomiya, and Funabashi 2009). These polymers offer similar properties to conventional plastics, but with the added advantage of being able to decompose naturally and safely in the environment.

One of the biodegradable thermoplastic polymers that has received considerable attention in recent years is poly(butylene succinate) (PBS). PBS is a semi-crystalline aliphatic thermoplastic polyester (Candal et al. 2020), synthetized by polycondensation between succinic acid (SA) and butanediol (BDO), resulting in a polybutylene chain with succinic acid ester bonds (Jiang and Zhang 2017; Rafiqah et al. 2021).

The importance of PBS lies in its ability to replace conventional plastics in applications where degradation is desirable or necessary, such as in single-use packaging, medical products, and agricultural applications. Furthermore, PBS offers suitable mechanical and thermal properties for manufacturing applications (Righetti et al. 2021).

Additive manufacturing is a set of technologies that allow the construction of 3D objects sequentially in a process of adding layers of material (plastic, metal, plaster). Among these techniques we can find the Fused Filament Fabrication (FFF), which is an additive manufacturing process used to produce parts with a complex geometry by the layer deposition of melted thermoplastic filaments (Brenken et al. 2018; Thézé et al. 2022).

The incorporation of biodegradable thermoplastic polymers, such as PBS, into the FFF process presents an exciting opportunity to enhance sustainability in additive manufacturing (Ahmadifar et al. 2021). While efforts have been made to optimize process parameters and address filament adhesion issues, the influence of crystallization on the internal structure and mechanical properties of 3D printed parts remains a critical area of study.

2. Bibliography review

2.1. Biodegradability of PBS

The degradation of PBS is influenced by various factors, such as molecular weight, water permeability, pH, temperature, purity, crystallinity, the presence of hydroxyl or carboxyl groups, and catalytic additives that may involve bacteria, enzymes, or inorganic fillers (Kitakuni et al. 2001). These factors play a crucial role in the degradation process and determine the rate and efficiency of PBS decomposition.

PBS can undergo degradation through methods such as hydrolytic degradation, enzymatic degradation, and biodegradation in environmental conditions like burial, activated sludge, and compost (Puchalski et al. 2018).

Studies have demonstrated that PBS exhibits a degradation rate of approximately 71.9% after 90 days, with PBS in powder form showing greater susceptibility to degradation compared to granules and films (Song & Qiu, 2009). Furthermore, research on PBS has revealed its biodegradability in various environments, including lipase solutions, soil burial, water, activated sludge, and compost. Notably, the natural degradation of PBS is initiated by enzymatic action, leading to its breakdown in the presence of water and CO2 (Anankaphong, Pentrakoon, and Junkasem 2015).

One of the most notable features of PBS is its ability to degrade under controlled environmental conditions, such as the presence of microorganisms and appropriate moisture levels. This degradation process occurs through the hydrolysis of the ester linkages, resulting in end products such as carbon dioxide, water, and metabolizable products by the microorganisms present in the environment (Kunioka, Ninomiya, and Funabashi 2009; Peñas et al. 2022).

Moreover, PBS exhibits effective decomposition into water and carbon dioxide (CO2), as previously mentioned. While PBS can be classified within fossil-based biodegradable polymers, recent advancements have focused on bio-based PBS. Despite its monomers (SA and BD) being primarily derived from petroleum, PBS and its copolymers exhibit biodegradability through natural enzymatic processes and microorganism action. Although there are several comprehensive reviews available discussing common

biodegradation pathways for biodegradable polymers like PCL, PLA, or PHAs (Brannigan and Dove 2017; Luyt and Malik 2019) relatively less information is currently available regarding the biodegradation of PBS due to ongoing research.

In summary, PBS represents an attractive option as a biodegradable thermoplastic polymer with suitable properties for additive manufacturing. Its ability to degrade under controlled environmental conditions and its potential for reducing the accumulation of persistent plastic waste make PBS a material of interest in the fields of sustainability and environmental protection.

2.2.PBS applications

The combination of mechanical, thermal, and biodegradable properties of PBS makes it a versatile material with a wide range of uses. Thanks to its transparency and robust construction, PBS offers a wide range of applications (Righetti et al. 2021). These applications encompass a wide range of sectors, as demonstrated by Figure 1. These include mulching films, compostable bags, nonwoven sheets and textiles, catering products, and foams (Li et al. 2005; Rafiqah et al. 2021).

Figure 1. PBS applications (Rafiqah et al. 2021)

Various researchers have noted that PBS is extensively used in industries such as agriculture, fishery, forestry, and civil engineering. In the agricultural sector, PBS is also

utilized for vegetation nets (Bautista et al. 2016). Additionally, PBS finds application in the manufacturing of monofilaments, injection-moulded products, tapes, split yarns, and textile industries (Rafiqah et al. 2021).

The processability of PBS is closely related to its molecular weight. For extrusion and injection moulding processes, a molecular weight below 100,000 is desirable, while higher molecular weights or long, branched chains are suitable for film blowing and casting techniques (Aliotta et al. 2022). Thermal stability and a high crystallization rate are critical for ensuring smooth processing. The addition of nucleating agents can enhance crystallinity and transparency (Kennouche et al. 2016).

In the context of food packaging applications, bioplastic materials like PBS are expected to provide protection and maintain the quality of the packaged food (Ngo et al. 2018). A study conducted by Siracusa et al., 2015 evaluated the behaviour and changes in permeability of PBS and PBSA films upon contact with food. The analysis revealed no significant damage to the materials, highlighting their potential in the food industry. Furthermore, recent advancements have introduced PBS reinforced with natural plant fibers, demonstrating the continuous development and market expansion of PBS-based materials (Mochane et al. 2021).

In summary, PBS and its derivatives have demonstrated versatility in various industries, including packaging, agriculture, fishery, forestry, construction, and electronics. The exceptional properties of PBS, combined with its processability and compatibility with other materials, enable its application in mulch films, packaging, dishware, foaming, drug encapsulation systems, orthopaedic applications, coffee capsules, and industrial settings. Notably, PBS has shown suitability for food packaging, ensuring food protection and quality maintenance. Ongoing research and development in PBS-based materials contribute to continuous innovation and further expansion of their market presence.

3. Materials and procedure

3.1. PBS

The Poly(butylene succinate), commonly known as PBS, is a thermoplastic and biodegradable aliphatic semi-crystalline polymer synthesized from succinic acid and 1,4-butanediol (Rafiqah et al. 2021). The chemical structure of PBS is illustrated in Figure 2.

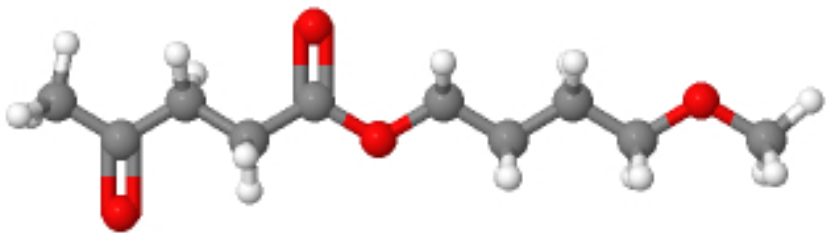

Figure 2. Chemical structure of PBS

The polymer used in our study is supplied by Naturplast (France) in the form of pellets and is denoted as PBE0003. It has a density of 1.26 g/cm^3 and a Melt Flow Index (MFI) of 4-6 g/10 min at 190 °C/2.16 Kg.

It is important to know the characteristics and properties of this material before working with it, as this data will be necessary for the subsequent analysis. Important values are listed in the table below.

Table 1. PBS properties

Property	Value	Reference
Density (g/cm^3)	1,26	Natureplast, 2021
T_g (°C)	-22	(Candal et al. 2020)
T_m (°C)	118	(Candal et al. 2020)
ΔH_m (J/g)	213	(Arandia et al. 2019)
% X_c	29	(Candal et al. 2020)

3.2. PBS films

For the first analysis with the optical microscope, PBS films were used, which were prepared using a thermo-pressing technique. The material used is a pellet of polymer and approximately 12 mg is needed, so it is necessary to cut a granule of typical mass 24

mg. Then the PBS pellet was placed in a vacuum chamber preheated for at least 1 hour to reach the temperature of 130 °C. A steel cylinder with a mass of 2 kg was placed on top of the pellet to allow melting and uniform squeezing of the material. The applied heat and pressure contributed to the transformation of the pellet into a flat, compact film.

Figure 3. Process of PBS film manufacturing

The photos depict the step-by-step process of film fabrication from the granules. The granule piece is initially positioned, followed by the placement of the weight on top. A Teflon sheet is inserted for easier peeling later. Once the duration has elapsed, the material is removed from the chamber and allowed to cool. The result is an approximately circular film with a diameter of around 2 cm and a thickness ranging from 50-70 µm.

3.3.Polarized Light Optical Microscopy

The morphological characterization of PBS will be performed using polarized light optical microscopy (PLOM). The Nikon LV-N100 microscope with polarized light is use, along with a Linkam hot stage THMS 600 to control the temperature. The objective of this experimental section is to study the growth rate of crystals at different temperatures.

Figure 4. Photographs of the Nikon LV-N100 microscope

For this study under the microscope, a PBS film is used, which will be placed between two glass plates. Firstly, an isothermal process will be conducted to eliminate the material's memory. This involves raising the temperature to 150 °C and maintaining it for 3 minutes. In this way, any previous crystal structure is ensured to be eliminated, providing a uniform starting point. The temperature is then reduced to the desired temperature and an extended isotherm of several hours is performed. The duration of this isotherm will depend on the specific temperature selected. As the temperature is increased, it has been observed that the time required for the appearance of crystals also increases. A total of 12 experiments were conducted, varying the temperature from 90 °C to 112 °C, with an increment of 2 degrees in each experiment.

During each experiment, continuous observations were made using the polarized light optical microscope, recording the times at which the crystals appeared at each temperature.

As mentioned earlier, the Linkam HMS600 heating stage is used to work with temperature changes and perform isothermal experiments. The stage is controlled using the LINK software, which allows programming of the previously described procedure with the required temperature stages.

For image capture, the Replay program is utilized. This program enables automatic image capture at desired time intervals. Furthermore, it offers the flexibility to adjust various image parameters, such as contrast, intensity, and others, to achieve the best possible resolution. Additionally, the image resolution can be adjusted according to the

different objectives available on the microscope, including magnifications of 100x, 50x, 25x, and 10x, to achieve the desired level of zoom.

In summary, the use of the Linkam heating stage, LINK software, and Replay program provides a comprehensive system for conducting thermal experiments and capturing images. This system enables precise control of temperature conditions and facilitates the analysis of growth rate trends. Through this methodology, we were able to investigate the growth rate of crystals systematically at different temperatures, gaining valuable insights into the observed results.

3.4. Differential Scanning Calorimetry (DSC)

To study the thermal properties of the material, Differential Scanning Calorimetry (DSC) will be employed. DSC is a thermo-analytical technique that measures the heat difference between a sample and a reference as a function of temperature (Piorkowska and Rutledge 2013). This thermal study allows us to gather information about the physical and chemical properties, as well as the transformations, of the sample when subjected to temperature variations. The DSC measurements will be conducted using the TA Instruments Q10 DSC, like the one shown in the photo. A cooling rate of 10 °C/min was used.

Figure 5. Photographs of DSC Q10

For sample analysis, aluminium crucibles have been used. After taring, a small amount of sample, between 2-3 mg of PBS sufficiently distributed over the surface, is introduced. The capsules are sealed with an aluminium lid. Once the capsule containing the sample

to be analysed is sealed, it is placed in the DSC alongside a reference capsule prepared in the same manner but left empty.

The sample was melted at 160 °C for 5 minutes to erase any thermal history, then cooled to the crystallization temperature (Tc) at a cooling rate of 10 °C/min and held at Tc until crystallization was completed. This process was performed for 7 crystallization temperatures ranging from 90 to 102 °C.

4. Results and discussion

4.1.Growth rate by PLOM

The size of the crystals is measured using PLOM images to determine their growth rate. In order to explain the procedure and the results obtained, the specific case of 90°C will be presented. For the other temperatures, the same steps are followed and the data are treated in a similar way. All tables and graphs will be included in the Annex, providing a complete overview of the results for each temperature.

The ImageJ software is utilized to measure the diameters of the most isolated crystals in each image as a function of time. As observed in the image sequence, two crystals are identified, and their respective diameters are measured.

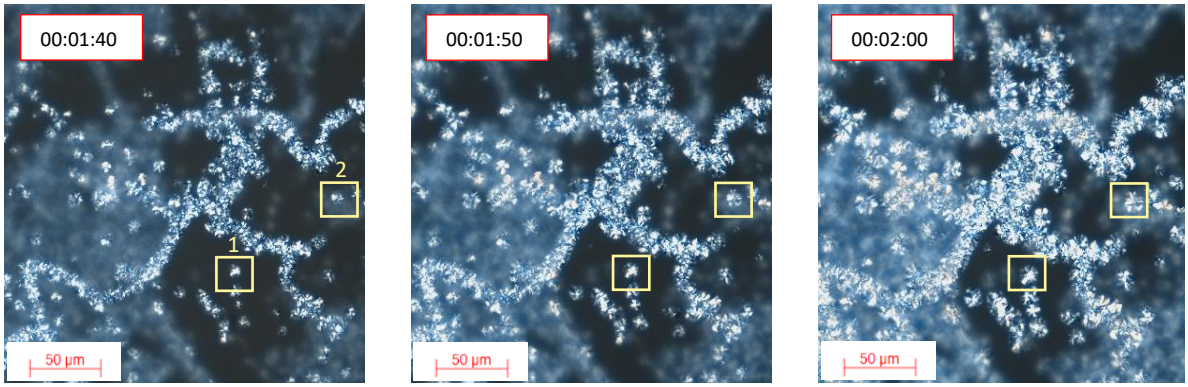

Figure 6. Sequence of image illustrating the crystal growth with 10 seconds intervals at 90 °C. At the top left corner, the time duration of the isothermal is indicated. The yellow squares indicate the isolated single crystals to be analysed.

The collected data is recorded and organized in a table for further analysis.

Table 2. Diameter values as a function of time for 90 °C

Crystal 1		Crystal 2	
Diameter (µm)	**Time (s)**	**Diameter (µm)**	**Time (s)**
8,273	0	9,152	0
10,843	5	11,905	5
13,926	10	14,086	10
16,239	15	16,790	15
18,448	20	18,860	20
21,737	25	24,204	25
25,334	30	27,095	30
26,593	35	28,875	35
29,445	40	31,755	40
31,064	45	35,668	45
		37,539	50
		40,617	55

After obtaining the diameter measurements of the crystals at different time points, the next step involves plotting these values on a graph. To determine the crystal growth rate, a trend curve is fitted to the data points on the graph. This curve represents the general linear trend or pattern of crystal growth over time. The slope of the trend curve represents the rate of growth of the crystal diameter with respect to time. For each case there will be two values, as two crystals have been measured. The average of the two shall then be taken. As can clearly be seen in the graph (Figure 7), the diameter increases with time.

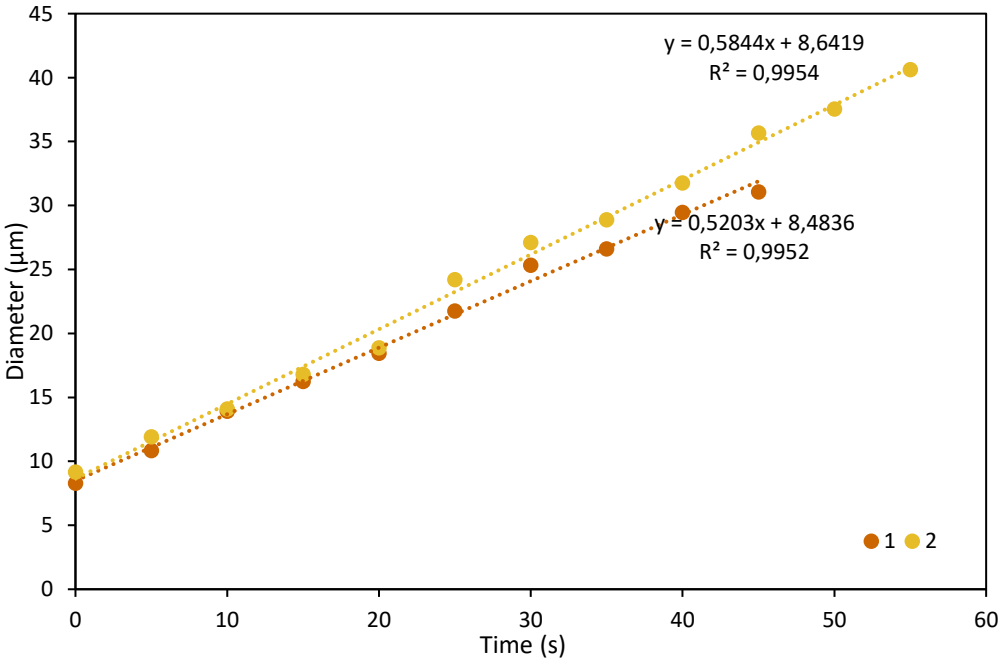

Figure 7. Diameter vs time for 90 °C

Measurements were carried out at different temperatures in the range of 90 °C to 112 °C. These measurements were carried out on two occasions. In the first series of measurements, the temperatures reached were not so high, going as low as 106 °C. This is because this first experience served as an introduction to the handling of the microscope and to become familiar with the times required. Subsequently, the process was repeated, this time reaching temperatures of up to 112 °C, which gives us two sets of data to analyse. The following Table 3 shows the velocity values obtained in both measurements.

Table 3. Growth rate values for each temperature of both tests

Temperature (°C)	Test 1		Test 2	
	G (mm/s)	G (µm/min)	G (mm/s)	G (µm/min)
90	6,40E-04	38,4	5,52E-04	33,14
92	4,22E-04	25,3	3,69E-04	22,17
94	2,90E-04	17,4	2,69E-04	16,12
96	1,85E-04	11,1	1,64E-04	9,85
98	1,55E-04	9,3	1,18E-04	7,06
100	1,28E-04	7,7	6,69E-05	4,02
102	7,38E-05	4,4	3,68E-05	2,21
104	3,45E-05	2,1	2,55E-05	1,53
106	2,91E-05	1,7	1,82E-05	1,09
108			9,76E-06	0,59
110			6,00E-06	0,36
112			2,43E-06	0,15

The correlation between growth rate and temperature in both experiments is shown below, compared to literature data from the study by Qiu and Yang's (Qiu and Yang 2006). Note the range of temperature in Qiu and Yang's results are lower than the present results presumably because the different PBS molecular weight (140 kg/mol versus 80 kg/mol for the present PBS according to the SEC report from Candal et al., 2020). Overall, the trend is similar with a strong decrease of the growth rate G as the temperature approached the melting temperature 115 °C.

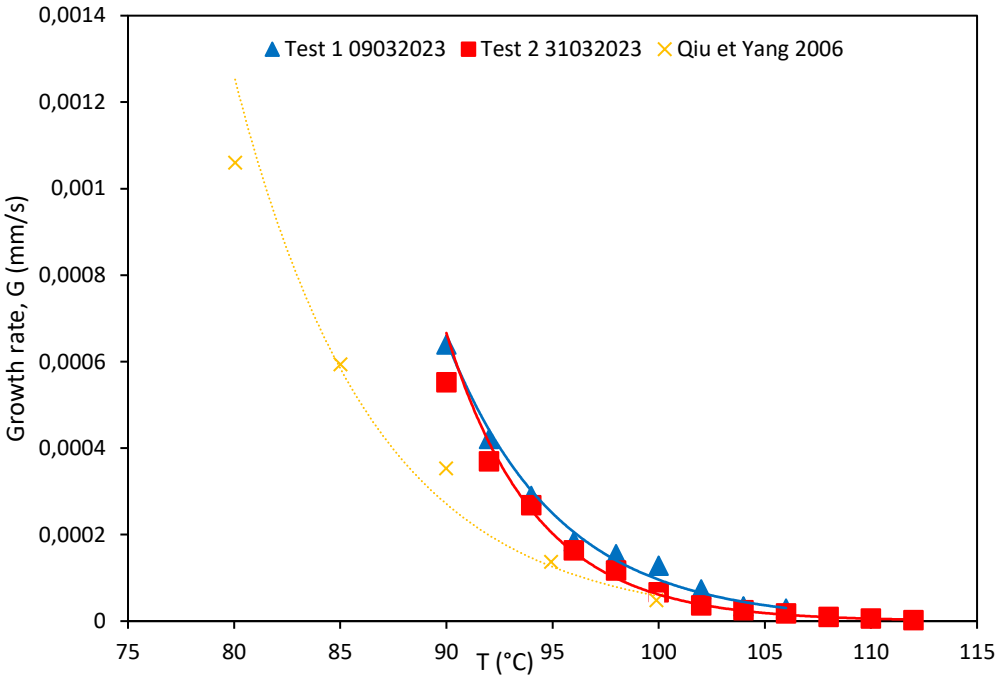

Figure 8. Spherulitic growth rate of PBS as a function of the isotherm temperature

4.2.Isothermal crystallization kinetics study by DSC

The isothermal melt crystallization kinetics of PBS was investigated with DSC. For this section, crystallization temperatures ranging from 90 °C to 102 °C were used, with an increment of 2 °C. Exothermic curves were recorded as a function of the crystallization time, from which the crystallization enthalpy (ΔH_c) was obtained. The variation of ΔH_c as a function of crystallization temperature is shown in Figure 9 (a) for PBS.

The value of ΔH_c increases from 31 J/g at 90 °C to 55 J/g at 102 °C. From this result, it can be said that the crystallisation temperature has an apparent effect on the enthalpy of crystallisation of PBS. This implies that at higher temperatures, more energy is required for the PBS molecules to form a stable crystalline structure.

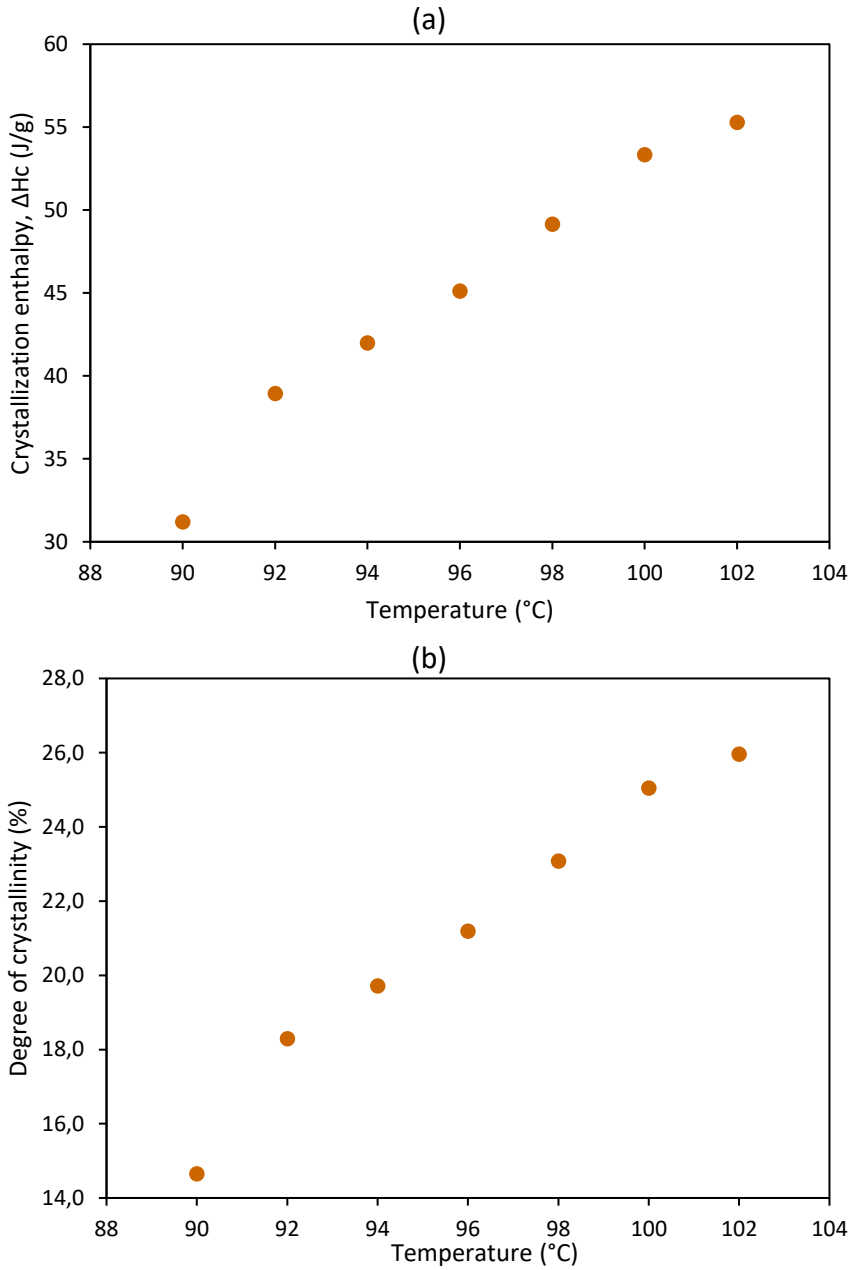

Figure 9. Crystallization temperature dependence of crystallization enthalpy (a) and crystallization temperature dependence of degree of crystallinity (b) for PBS

From these results, the degree of crystallinity can be determined, which is defined using the following equation (Candal et al. 2020):

$$X_c = \frac{\Delta H_m}{\Delta H_m^o} \cdot 100 \qquad (1)$$

where ΔH_m (J/g) is the melting enthalpy of the sample and ΔH_m^o is the melting enthalpy of a 100% crystalline polymer. It is taken as bibliographic value from Arandia et al., 2019 ΔH_m^o = 213±10 J/g.

Therefore, using the above equation and the data provided in Figure 9 (a), the calculation of the degree of crystallinity for each of the temperatures was performed and the results are shown in Figure 9 (b).

Figure 9 (b) represents the degree of crystallinity as a function of crystallization temperature. It is observed that as the crystallization temperature increases, the degree of crystallinity also increases. The degree of crystallinity of PBS increases from approximately 14% to 26% when the temperature is increased from 90 °C to 102 °C.

Both curves exhibit a similar trend, but the percentage increase in the degree of crystallinity is lower compared to the enthalpy. This indicates that while the crystallization temperature has a noticeable effect on both the degree of crystallinity and the enthalpy, the degree of crystallinity shows a relatively smaller change compared to the enthalpy.

By assuming that the change in crystallinity is directly related to the change in heat release during crystallization, we can determine the relative degree of crystallinity, X(t), using the following equation (Papageorgiou, Achilias, and Bikiaris 2007),

$$X(t) = \frac{\int_0^t \left(\frac{dH_c}{dt}\right) dt}{\int_0^\infty \left(\frac{dH_c}{dt}\right) dt} \qquad (2)$$

where dH_c represents the measured enthalpy of crystallization during an infinitesimal time interval dt. The limits t and ∞ are used to indicate the elapsed time during crystallization and at the end of the crystallization process, respectively.

Figure 10 illustrates the relation between relative crystallinity and crystallization time for PBS at different crystallization temperatures (Tc). It can be observed that as the Tc value increases, the crystallization time becomes longer. This phenomenon indicates that the crystallization process is delayed at higher Tc values, resulting in slower crystal growth and lower overall crystallinity.

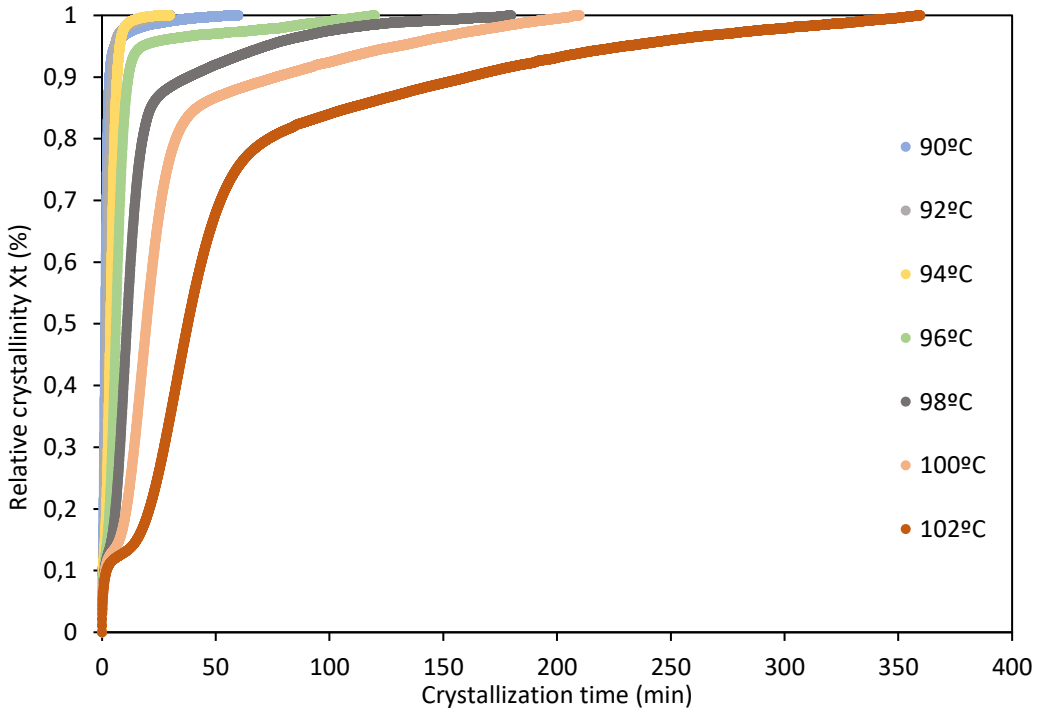

Figure 10. Development of relative crystallinity with crystallization time at indicated Tc

In the following, the Avrami equation (3) is used to analyse the overall isothermal crystallisation of PBS. (3) is a mathematical model that describes the rate of crystal growth during a crystallization process, in other words, it usually applied to analyse the kinetics of isothermal crystallization (Lorenzo et al. 2007; Zhan et al. 2014). It assumes that the relative degree of crystallinity $X(t)$ develops as a function of crystallization time t, so that the equation is expressed as follows (Krevelen and Nijenhuis 2009),

$$X(t) = 1 - exp(-Kt^n) \qquad (3)$$

It can be also written as

$$ln\left[-ln\left[1 - X(t)\right]\right] = n\, ln\, t + ln\, K \qquad (4)$$

in this way the constants n and K may be obtained by plotting $ln\left[-ln\left[1 - X(t)\right]\right]$ vs. $ln\, t$ as shown in Figure 11.

To obtain these curves, a prior data analysis has been conducted, where not all data points are considered. Instead, a specific range is selected. The analysis starts from $X(t) = 0.2$ and extends up to approximately $X(t) = 0.9$ as the upper limit. This decision

is based on the observation in Figure 10, where the crystallinity values start to be significant from this point onwards.

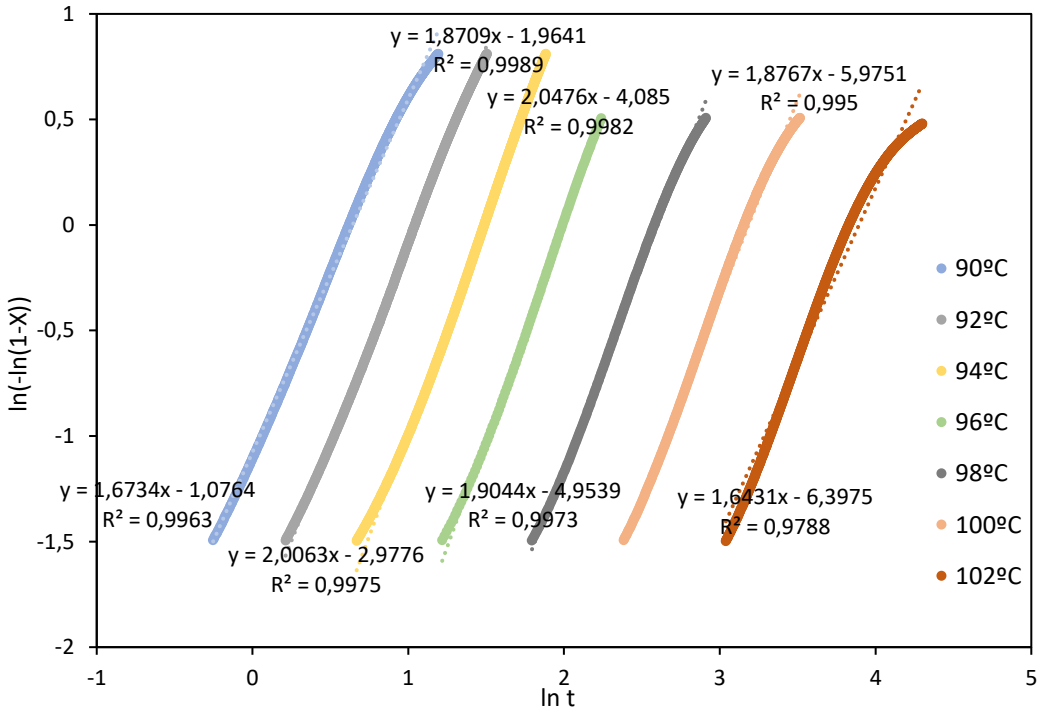

Figure 11. Avrami plots for each temperature and with its respective trend line

The results presented in Figure 11 demonstrate a series of nearly linear plots obtained for the samples crystallized at different Tc values. This observation suggests that the Avrami method is suitable for describing the isothermal melt crystallization process in these samples.

From each trend curve, the values of n and K are obtained by determining the slope and the y-intercept, respectively, for all temperature values. PBS kinetic data are summarised in Table 4.

Table 4. Parameters k, n, t_{max} and $t_{1/2}$ from the Avrami analysis

Tc (°C)	k (min^{-n})	n	t_{max} (min)	$t_{1/2}$
90	3,41E-01	1,67	1,1044	1,5284
92	1,40E-01	1,87	1,8986	2,3489
94	5,09E-02	2,01	3,1274	3,6746
96	1,68E-02	2,05	5,3001	6,1473
98	7,06E-03	1,90	9,1186	11,1216
100	2,54E-03	1,88	16,0913	19,8568
102	1,67E-03	1,64	27,7335	39,2704

It is observed that the values of n in this study vary between 1,6 and 2. When comparing these data with the studies of Qiu & Yang, 2006 and Dai & Qiu, 2017 a small difference is noted, since in both publications the values hardly vary and are around 2.6 and 2.8. These values close to 3 indicate that the crystallisation of PBS may correspond to three-dimensional growth in the form of a truncated sphere, as indicated in Figure 12 (Krevelen and Nijenhuis 2009). Although similar values of n were not obtained in this study and vary considerably, as will be developed in the next section where the crystalline morphology is analysed by PLOM, a consistent spherulite morphology is maintained for all temperatures studied, independently of the value of n.

Likewise, as the crystallisation temperature increases, the k values show a decreasing trend, indicating the suppression of crystallisation at higher temperatures.

	Type of nucleation			
	Predetermined (constant number of nuclei per cm)		Spontaneous (sporadic) (constant nucleation rate)	
Form of growth	n	K	n	K
Spherulitic (spheres)	3	$\frac{4}{3}\pi v^3 N\rho*$	4	$\frac{1}{3}\pi v^3 J\rho*$
Discoid (platelets)	2	$\pi b v^2 N\rho*$	3	$\frac{1}{3}\pi b v^2 J\rho*$
Fibrillar (rodlets)	1	$fvN\rho*$	2	$\frac{1}{2}fvJ\rho*$

b = thickness of platelet; f = cross section of rodlet; ρ^* = relative density ρ_c/ρ; N = number of nuclei per unit volume; J = rate of nucleation per unit volume; v = rate of crystal growth.

Figure 12. Constants n and K of Avrami equation (Krevelen and Nijenhuis 2009)

t_{max} represents the point at which dQ/dt ($Q(t)$ being the heat flow), is equal to zero, it can be expressed in terms of the variables n and k as follows:

$$t_{max} = \left(\frac{n-1}{nk}\right)^{1/n} \qquad (5)$$

From the values of k and n given in the Table 4, the corresponding values of t_{max} can be calculated, which are also presented in the Table 4. It is evident that the higher the crystallisation temperature, the higher the value of t_{max}.

The half-life crystallization time ($t_{1/2}$) represents the time required to reach half of the final crystallinity (Xt = 0.5). It is an important parameter for discussing crystallization kinetics. It is calculated using the following equation:

$$t_{1/2} = \left(\frac{\ln 2}{k}\right)^{1/n} \qquad (6)$$

And the values are shown in the Table 4. Figure 13a present the plots of $t_{1/2}$ against Tc.

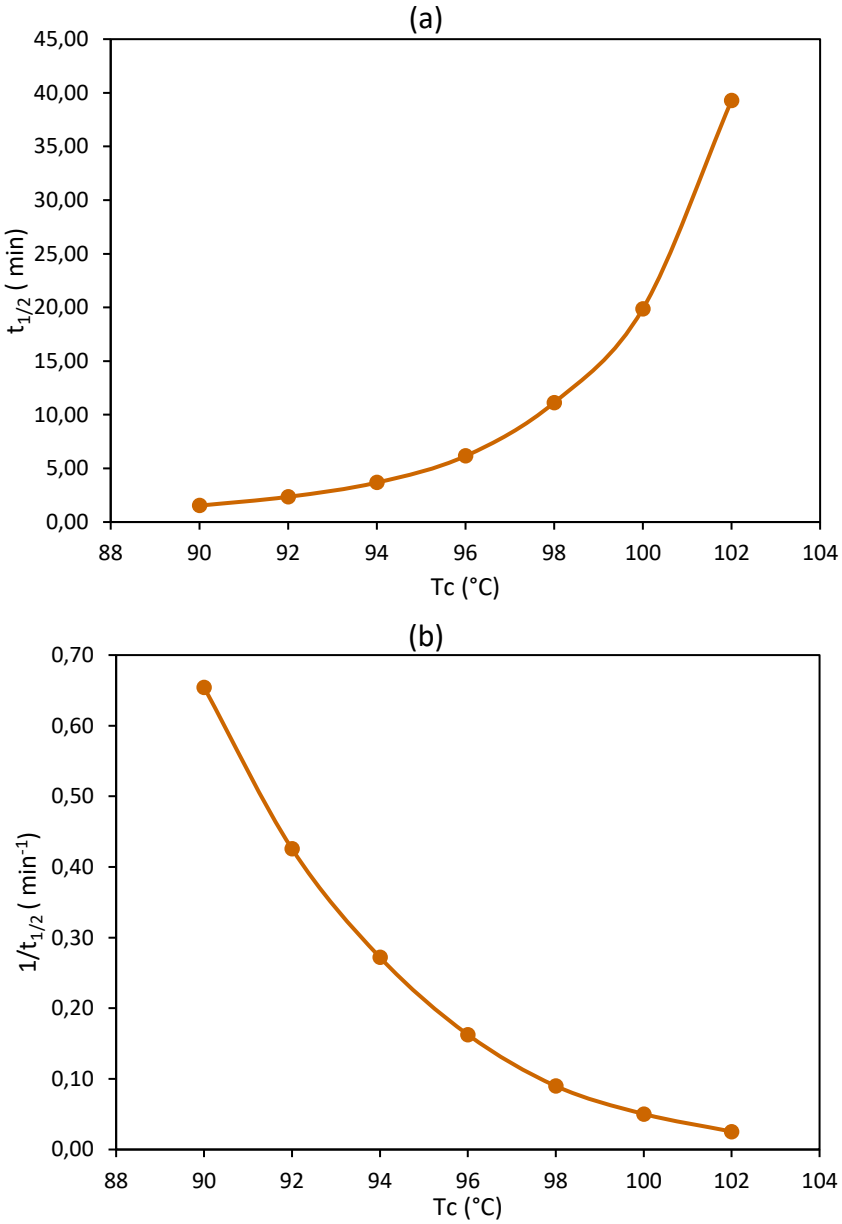

Figure 13. Variations of $t_{1/2}$ (a) and of $1/t_{1/2}$ (b) with temperature (Tc)

For all points, $t_{1/2}$ increases with increasing temperature, indicating that the overall crystallisation rate became slower at higher Tc. This observation suggests that the overall rate of crystallization decreased at higher Tc. This phenomenon is commonly observed in polymer crystallization and can be attributed to the difficulty of nucleation, which plays a crucial role in determining the overall crystallization rate of a polymer

undergoing melt crystallization at temperatures close to the melting point (Tm). In contrast, the value of $1/t_{1/2}$ exhibits a decrease as the crystallization temperature increases. The trend of both curves is the same but in reverse.

4.3.Spherulitic morphology by PLOM

In this study, a detailed analysis of the spherulitic morphology and growth rate of PBS crystals was carried out. Using PLOM with a hot stage to study the behaviour of PBS over a wide range of crystallisation temperatures, varying from 90 °C to 112 °C, as detailed in the previous sections.

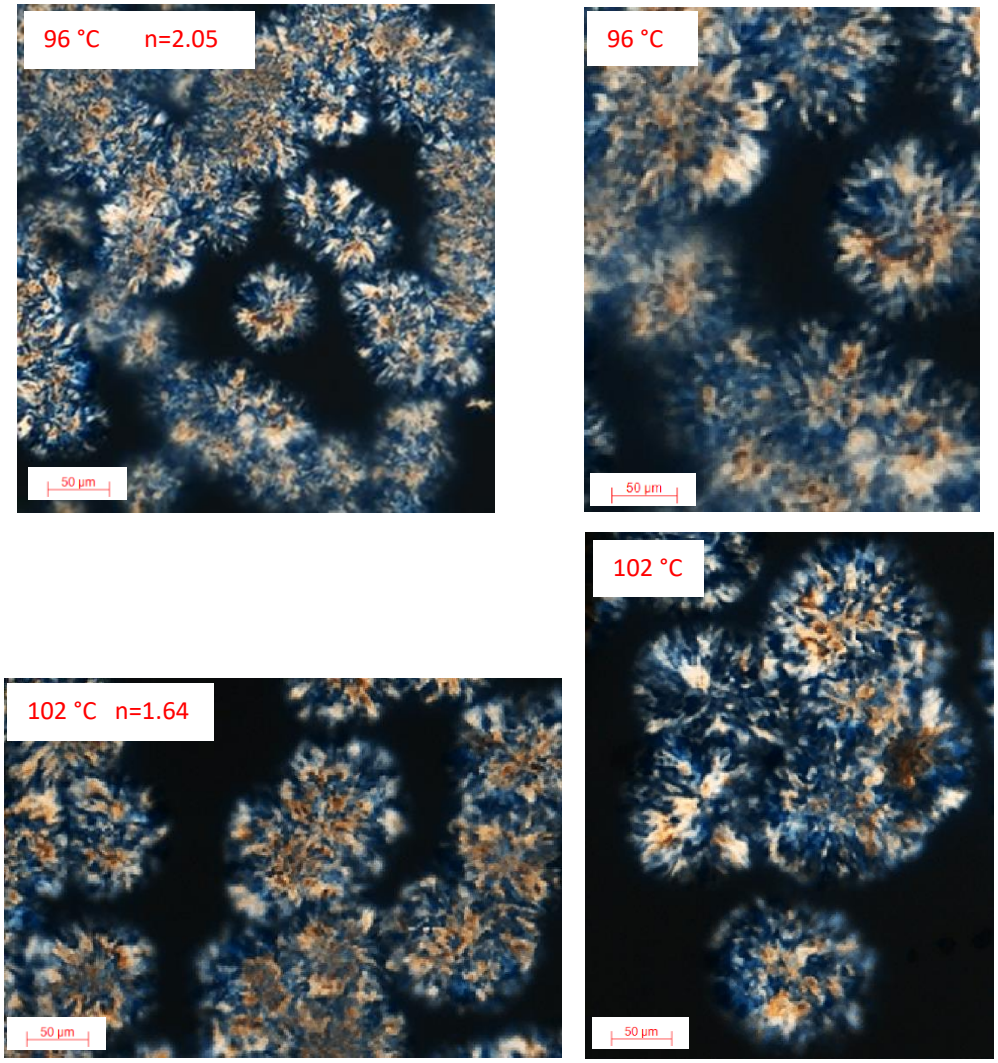

Figure 14. Optical micrographs of the spherulitic morphology of PBS crystallized at various temperatures.

As mentioned previously, given the variability in the n values obtained, it is interesting to examine the images obtained at different temperatures to determine whether these

differences in n are also reflected in different crystal structures. For this purpose, two representative temperatures were selected: the temperature with the highest n-value, which corresponds to 96 °C, and the temperature with the lowest n-value, which is 102 °C.

The images in Figure 14 clearly show that there is no structural difference between the PBS crystals at 102 °C and 96 °C, despite the variation in n values. At all temperatures studied, the morphology of the crystals is clearly identified as dendritic spherulites.

To obtain a better view of the crystals, images were taken at a crystallisation temperature of 106 °C (Figure 15). In this case, efforts were made to capture the most isolated crystals and capture the images with maximum zoom. This allowed for greater clarity in the shape and structure of the crystals.

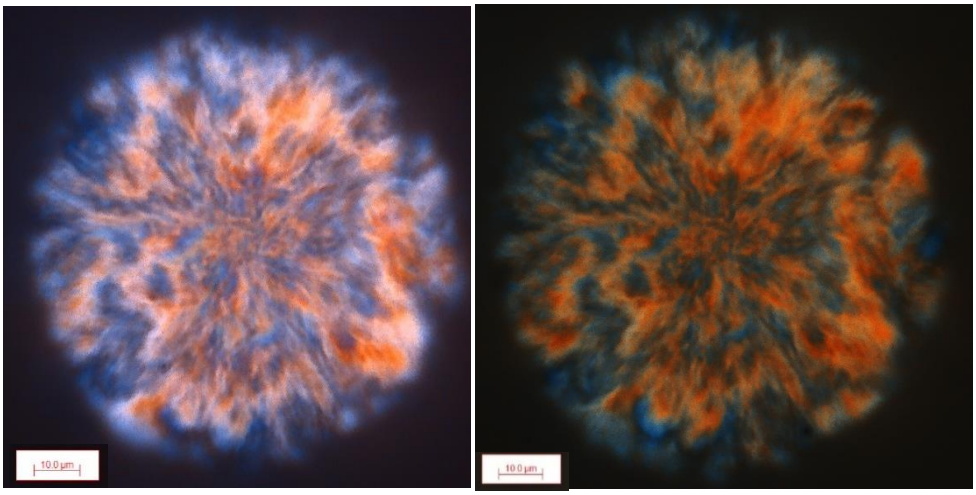

Figure 15. Polarized light optical micrographs for PBS at 106 °C

5. Conclusions

Throughout this study, a comprehensive investigation has been conducted to explore the kinetics of isothermal crystallization during melting, analyse crystal growth rates, and examine spherulitic morphology in depth. Various techniques were employed, and multiple experiments were performed to ensure reliable and meaningful data, culminating in the following noteworthy conclusions.

The growth rate and spherulitic morphology were meticulously studied using PLOM with a heating plate, encompassing a crystallization temperature range from 90 °C to 106 °C. The findings demonstrated that as the temperature increased, the crystal growth rate exhibited a notable decrease. On the other hand, the images clearly depict the spherulitic morphology of PBS crystals. They exhibit a dendritic shape, resembling branched structures extending from a central core.

The study of the isothermal crystallisation kinetics of PBS was carried out using Differential Scanning Calorimetry (DSC), and a detailed analysis was performed by applying the Avrami equation. For this study, measurements were taken in a temperature range from 90 °C to 102 °C. It has been observed that the degree of crystallinity increases with increasing temperature.

Furthermore, the relationship between relative crystallinity and crystallization time of PBS at different crystallization temperatures (Tc) has been examined, leading to the conclusion that as the Tc value increases, the crystallization time extends. This indicates that the crystallization process is delayed at higher Tc values, resulting in slower crystal growth.

Additionally, the coefficients n and k were obtained from the Avrami plots. Regarding the values of k, they decrease as the temperature increases, indicating a slowdown in crystallization at higher temperatures. The values of n vary between 1.6 and 2, suggesting a potential difference in crystal structures at these temperatures. However, as observed in the PLOM images, there is no discernible difference. This variation in n values could be attributed to experimental errors, such as a low sample mass of PBS.

In summary, this study provided a deeper understanding of the isothermal crystallisation kinetics, growth rates and spherulitic morphology of PBS crystals. An inverse relationship between crystallisation temperature and crystal growth rate was observed, as well as a consistent spherulitic morphology at all temperatures studied. However, there are still open questions that could be the subject of future research.

In relation to FFF additive manufacturing, an important aspect that could be explored in future research is the effect of cooling temperature on crystal growth during the solidification process of the printed material. As the part cools down after the deposition of the molten filament, crystals could grow and develop their structure. The cooling rate can significantly influence the size and orientation of the crystals, which in turn can affect the mechanical and thermal properties of the printed parts.

REFERENCES

Ahmadifar, M., K. Benfriha, M. Shirinbayan, and A. Tcharkhtchi. 2021. 'Additive Manufacturing of Polymer-Based Composites Using Fused Filament Fabrication (FFF): A Review'. *Applied Composite Materials* 28(5): 1335–80.

Aliotta, Laura et al. 2022. 'A Brief Review of Poly (Butylene Succinate) (PBS) and Its Main Copolymers: Synthesis, Blends, Composites, Biodegradability, and Applications'. *Polymers* 14(4): 844.

Anankaphong, Hemhong, Duanghathai Pentrakoon, and Jirawut Junkasem. 2015. 'Effect of Rubberwood Content on Biodegradability of Poly(Butylene Succinate) Biocomposites'. *International Journal of Polymer Science* 2015: 1–9.

Arandia, Idoia et al. 2019. 'Tailoring the Isothermal Crystallization Kinetics of Isodimorphic Poly (Butylene Succinate-Ran-Butylene Azelate) Random Copolymers by Changing Composition'. *Polymer* 183: 121863.

Bautista, Mayka et al. 2016. 'Cationic Poly(Butylene Succinate) Copolyesters'. *European Polymer Journal* 75: 329–42.

Brannigan, Ruairí P., and Andrew P. Dove. 2017. 'Synthesis, Properties and Biomedical Applications of Hydrolytically Degradable Materials Based on Aliphatic Polyesters and Polycarbonates'. *Biomaterials Science* 5(1): 9–21.

Brenken, Bastian et al. 2018. 'Fused Filament Fabrication of Fiber-Reinforced Polymers: A Review'. *Additive Manufacturing* 21: 1–16.

Candal, María Virginia et al. 2020. 'Thermo-Rheological Effects on Successful 3D Printing of Biodegradable Polyesters'. *Additive Manufacturing* 36: 101408.

Dai, Xun, and Zhaobin Qiu. 2017. 'Crystallization Kinetics, Morphology, and Hydrolytic Degradation of Novel Biobased Poly(Butylene Succinate- Co -Decamethylene Succinate) Copolyesters'. *Polymer Degradation and Stability* 137: 197–204.

Jiang, Long, and Jinwen Zhang. 2017. 'Biodegradable and Biobased Polymers'. In *Applied Plastics Engineering Handbook*, Elsevier, 127–43. https://linkinghub.elsevier.com/retrieve/pii/B9780323390408000079 (June 6, 2023).

Kennouche, Salima et al. 2016. 'Morphological Characterization and Thermal Properties of Compatibilized Poly(3-Hydroxybutyrate-Co-3-Hydroxyvalerate) (PHBV)/Poly(Butylene Succinate) (PBS)/Halloysite Ternary Nanocomposites'. *European Polymer Journal* 75: 142–62.

Kitakuni, Eiichi et al. 2001. 'Biodegradation of Poly(Tetramethylene Succinate-Cotetramethylene Abdicate) and Poly(Tetramethylene Succinate) through

Water-Soluble Products'. *Environmental Toxicology and Chemistry* 20(5): 941–46.

Krevelen, D. W. van, and K. te Nijenhuis. 2009. *Properties of Polymers: Their Correlation with Chemical Structure: Their Numerical Estimation and Prediction from Additive Group Contributions*. 4th, completely rev. ed ed. Amsterdam: Elsevier.

Kunioka, Masao, Fumi Ninomiya, and Masahiro Funabashi. 2009. 'Biodegradation of Poly(Butylene Succinate) Powder in a Controlled Compost at 58 °C Evaluated by Naturally-Occurring Carbon 14 Amounts in Evolved CO2 Based on the ISO 14855-2 Method'. *International Journal of Molecular Sciences* 10(10): 4267–83.

Li, Haiyan, Jiang Chang, Amin Cao, and Junying Wang. 2005. 'In Vitro Evaluation of Biodegradable Poly(Butylene Succinate) as a Novel Biomaterial'. *Macromolecular Bioscience* 5(5): 433–40.

Lorenzo, Arnaldo T., María Luisa Arnal, Julio Albuerne, and Alejandro J. Müller. 2007. 'DSC Isothermal Polymer Crystallization Kinetics Measurements and the Use of the Avrami Equation to Fit the Data: Guidelines to Avoid Common Problems'. *Polymer Testing* 26(2): 222–31.

Luyt, Adriaan S., and Sarah S. Malik. 2019. 'Can Biodegradable Plastics Solve Plastic Solid Waste Accumulation?' In *Plastics to Energy*, Elsevier, 403–23. https://linkinghub.elsevier.com/retrieve/pii/B9780128131404000169 (June 6, 2023).

Mochane, Mokgaotsa J., Sifiso I. Magagula, Jeremia S. Sefadi, and Teboho C. Mokhena. 2021. 'A Review on Green Composites Based on Natural Fiber-Reinforced Polybutylene Succinate (PBS)'. *Polymers* 13(8): 1200.

Ngo, Tuan D. et al. 2018. 'Additive Manufacturing (3D Printing): A Review of Materials, Methods, Applications and Challenges'. *Composites Part B: Engineering* 143: 172–96.

Papageorgiou, George Z., Dimitris S. Achilias, and Dimitris N. Bikiaris. 2007. 'Crystallization Kinetics of Biodegradable Poly(Butylene Succinate) under Isothermal and Non-Isothermal Conditions'. *Macromolecular Chemistry and Physics* 208(12): 1250–64.

Peñas, Mario Iván, Ricardo Arpad Pérez-Camargo, Rebeca Hernández, and Alejandro J. Müller. 2022. 'A Review on Current Strategies for the Modulation of Thermomechanical, Barrier, and Biodegradation Properties of Poly (Butylene Succinate) (PBS) and Its Random Copolymers'. *Polymers* 14(5): 1025.

Piorkowska, Ewa, and Gregory Charles Rutledge, eds. 2013. *Handbook of Polymer Crystallization*. Hoboken, New Jersey: Wiley.

Puchalski, Michał et al. 2018. 'Molecular and Supramolecular Changes in Polybutylene Succinate (PBS) and Polybutylene Succinate Adipate (PBSA) Copolymer during Degradation in Various Environmental Conditions'. *Polymers* 10(3): 251.

Qiu, Zhaobin, and Wantai Yang. 2006. 'Crystallization Kinetics and Morphology of Poly(Butylene Succinate)/Poly(Vinyl Phenol) Blend'. *Polymer* 47(18): 6429–37.

Rafiqah, S. Ayu et al. 2021. 'A Review on Properties and Application of Bio-Based Poly(Butylene Succinate)'. *Polymers* 13(9): 1436.

Righetti, Maria Cristina, Maria Laura Di Lorenzo, Patrizia Cinelli, and Massimo Gazzano. 2021. 'Temperature Dependence of the Rigid Amorphous Fraction of Poly(Butylene Succinate)'. *RSC Advances* 11(41): 25731–37.

Siracusa, Valentina, Nadia Lotti, Andrea Munari, and Marco Dalla Rosa. 2015. 'Poly(Butylene Succinate) and Poly(Butylene Succinate-Co-Adipate) for Food Packaging Applications: Gas Barrier Properties after Stressed Treatments'. *Polymer Degradation and Stability* 119: 35–45.

Song, Liang, and Zhaobin Qiu. 2009. 'Crystallization Behavior and Thermal Property of Biodegradable Poly(Butylene Succinate)/Functional Multi-Walled Carbon Nanotubes Nanocomposite'. *Polymer Degradation and Stability* 94(4): 632–37.

Thézé, Alexis et al. 2022. 'Fused Filament Fabrication Process Window for Good Interlayer Bonding: Application to Highly Filled Polymers in Metallic Powder*'. *Polymer Engineering & Science* 62(2): 336–48.

Zhan, Jing et al. 2014. 'Crystallization and Melting Properties of Poly(Butylene Succinate) Composites with Titanium Dioxide Nanotubes or Hydroxyapatite Nanorods'. *Journal of Applied Polymer Science* 131(11): n/a-n/a.